water

MDPI

Article

Enhancing Hydraulic Efficiency of Side Intakes Using Spur Dikes: A Case Study of Hemmat Water Intake, Iran

Saman Abbasi Chenari [1], Hossein Azizi Nadian [2], Javad Ahadiyan [3,4], Mohammad Valipour [5,*], Giuseppe Oliveto [6,*] and Seyed Mohsen Sajjadi [3,4]

1 Department of Water Sciences and Environmental Research Center, Islamic Azad University, Shoushtar Branch, Shoushtar 64517-41117, Iran; samanabasi@yahoo.com
2 Department of Civil Environmental Architectural Engineering and Mathematics, University of Brescia, Via Branze 43, 25123 Brescia, Italy; hossein.azizinadian@unibs.it
3 Faculty of Water and Environmental Engineering, Shahid Chamran University of Ahvaz, Ahvaz 61357-83151, Iran; j.ahadiyan@scu.ac.ir (J.A.); m.sadjadi@scu.ac.ir (S.M.S.)
4 Center of Excellence of the Irrigation and Drainage Networks Improvement and Maintenance, Golestan Blvd, Ahvaz 61357-43311, Iran
5 Department of Engineering and Engineering Technology, Metropolitan State University of Denver, Denver, CO 80217, USA
6 School of Engineering, University of Basilicata, Viale dell'Ateneo Lucano 10, 85100 Potenza, Italy
* Correspondence: mvalipou@msudenver.edu (M.V.); giuseppe.oliveto@unibas.it (G.O.)

Abstract: This study investigates the problem of low efficiency and the lack of a water supply at the Hemmat Water Intake, in Iran, where severe sediment accumulation was observed at the intake mouth. The Flow-3D software was used to simulate the flow patterns under various scenarios of hydraulic regimentation works. The considered parameters include: (i) three alternative locations of the spur dike (i.e., a spur dike placed on the opposite side of the intake inlet and aligned with the upstream edge of the intake, to be regarded as a witness spur dike; a spur dike at a distance D_S of 7 m downstream of the witness spur dike, which implies a dimensionless distance D_S/b_{i1} of 1/3, with b_{i1} being the intake opening width; and a spur dike at a distance of 7 m upstream of the witness spur dike with a dimensionless distance, still, of 1/3); (ii) four spur dike lengths, L_S/B_r, with L_S being the effective spur dike length and B_r the approach river width; and (iii) five spur dike deviation angles of 75, 90, 105, 120, and 135 degrees (the deviation angle is the angle between the spur dike axis and the original river-bank line from which the spur dike extends). The results showed that, with the increase in the relative spur dike length (L_S/B_r), the velocity of the flow entering the water intake increases by 11%. A spur deviation angle of 135 degrees increases the flow depth at the intake inlet by 9% compared to a smaller deviation angle of 75 degrees. In addition, the spur dike increases the flow shear stresses at the intake inlet by up to 50%. Overall, the main flow of the river with the highest velocity and depth, and best directed towards the water intake, occurs for the placement of the longest spur dike (i.e., $L_S/B_r = 0.46$) in front of the inlet (i.e., witness spur dike) and for a spur dike deviation angle of 135 degrees. The spur dike increases the shear stress at the intake entrance by more than five times with respect to the case of its absence. In general, the presence of a spur dike on the opposite bank and with a deviation angle in the direction of the intake inlet well directs the main flow towards the canal intake. Moreover, it reduces the possibility of sedimentation in the canal inlet by increasing the flow velocity. Therefore, the results of this study could also be useful in increasing the hydraulic efficiency of lateral intakes by reducing the sedimentation phenomena.

Keywords: diversion channels; Flow-3D software; hydraulic efficiency; side intakes; spur dike

check for updates

Citation: Chenari, S.A.; Nadian, H.A.; Ahadiyan, J.; Valipour, M.; Oliveto, G.; Sajjadi, S.M. Enhancing Hydraulic Efficiency of Side Intakes Using Spur Dikes: A Case Study of Hemmat Water Intake, Iran. *Water* **2024**, *16*, 2254. https://doi.org/10.3390/w16162254

Academic Editors: Vlassios Hrissanthou, Mike Spiliotis and Konstantinos Kaffas

Received: 31 May 2024
Revised: 5 August 2024
Accepted: 7 August 2024
Published: 9 August 2024

Copyright: © 2024 by the authors. Licensee MDPI, Basel, Switzerland. This article is an open access article distributed under the terms and conditions of the Creative Commons Attribution (CC BY) license (https://creativecommons.org/licenses/by/4.0/).

1. Introduction

Lateral intakes are hydraulic structures that divert water from rivers for domestic, agricultural, and industrial purposes [1]. The structure and performance of the water

intake structures lead, in their vicinity, to the deviation of the streamlines near them, which, together with the flow-pressure gradient and centrifugal forces, leads to the formation of some vortices at the structure entrance, creating complex three-dimensional flow patterns at lateral intakes [2]. At any time, the condition of a water supply with a maximum (diverted) discharge and minimal settling should be considered as the optimal operating condition for an intake structure [3,4]. Determining the intake flow depth is one of the most important issues in lateral intake design, and affects the diversion flow ratio [5]. However, artificial structures such as spur dikes can increase the water intake efficiency and reduce sedimentation loads [6,7]. Intake structures also have some disadvantages, such as flow separation in the upstream wall of the intake channel, the generation of secondary currents and eddies that prevent the flow from entering the intake channel, and the formation of a stagnant flow area prone to the settling of sediments near the outer wall, causing a reduction in the width of the passing flow and the efficiency of the intake [8–10]. Moreover, the flow diverted toward the intake leads to changes in the hydraulic conditions and distribution of the flow velocity in the river and at the intake inlet [6,7]. Therefore, a complete understanding of the processes that occur after intake construction can help to optimize the water diversion mechanism and improve the performance of the intake structures. Below, a short review on various research studies focused on increasing the hydraulic efficiency of lateral intakes is presented.

Some researchers have suggested some key points to increase the efficiency of lateral intakes. As examples: the use of a 90-degree water intake, the application of intakes with different angles, and placing the intake location on the outer bend of the river. However, many of these configurations need to be analyzed especially with numerical models. Abolghasemi et al. [11] evaluated water intakes with 90- and 52-degree angles. They reported that water intakes with a 52-degree deviation angle exhibit better efficiency with regard to the transfer of sediment and return flows at the water intakes. Kashyap et al. [12] showed the entrainment sediment capacity of the flow depending on the positions and sizes of regions of high bed shear stress. Azimi et al. [13] discovered that a secondary circulation cell develops downstream of the intake channel based on the simulation results for lateral intakes with a vertical diversion. Montaseri et al. [2] investigated a 90-degree-angle water intake in a 180-degree river bend. They concluded that sedimentation would occur along the inner bound curve if they installed the intake structure in the second half of the bend. On the other hand, if the intake were placed in the first half of the bend, sediments would accumulate along both the inner and outer bounders of the bend, and more sediments would enter the intake.

Based on a laboratory study on lateral intakes in a 180-degree bend, Masjedi and Foroushani [5] showed that the intake discharge ratio is directly related to the increase in flow depth. In branching channel flow, the discharge ratio is the ratio between the branch channel discharge and the main channel upstream discharge. Jalili et al. [9], using a laboratory study and the Sediment Simulation in Intakes with Multiblock option (SSIIM) model, showed that the amount of sediments entering an intake increases with an increase in the intake–discharge ratio. Babagoli Sefidkoohi et al. [14] concluded that the Re-Normalisation Group (RNG) turbulence model in Flow-3D leads to results with a minimal error in flow simulations in a river with lateral intakes. Safarzadeh and Khaiatrostami [15] concluded that, along the diversion channel, the presence of highly turbulent dividing surfaces induces an instability of shear layers matched by strong instantaneous vertical motions and, consequently, bed shear stresses. Tavakoli et al. [16] considered laboratory and numerical models of lateral intakes in 180-degree bends. They showed that the minimum sediment load entering the intake occurs for an intake deviation angle of 50 degrees, and the best location of the intake in the bend is at an angle of 120 degrees for all discharge ratios. In addition, Sayed [17] showed, in his experimental work, that the largest discharge ratio occurs at the branching angle of 45 degrees, while the smallest at the branching angle of 90 degrees. Moreover, the laboratory results by Alomari et al. [4] showed that reducing the intake diversion angle would lead to a reduction in sediment

transport in the diversion channel; a 30-degree diversion angle can reduce the sediment transport by up to 64%. Heidari Rad et al. [18] concluded that, when diverging the flume to sizes of 0.75 and 0.50, the diversion sediment to the intake decreased by 35.4 and 49.9%, respectively. They also compared the experimental results to those from CCHE2D (i.e., an integrated software package developed at the National Center for Computational Hydroscience and Engineering, the University of Mississippi) and Flow-3D numerical models, noting good accuracy. The models founds that the diversion flow decreases by 21.9 and 31.8%, respectively. Furthermore, Montaseri et al. [2], using the Ansys Fluent (version 6.2) software, showed that sedimentation occurs along the inner bank of a bend and enters the intake, from the downstream edge, in the case of intakes in the second half of the bend. Still considering research based on three-dimensional flow simulations, Meshkati and Salehi [19] found that the modelling errors in the main channel and intake were about 7.3% and 19.7%, respectively, when considering lateral intakes in a 180-degree bend. Niknezhad et al. [20] concluded that the RNG turbulence model is more accurate than the standard k-ε turbulence model.

Various structures, including submerged plates and vanes, are used to increase the efficiency of lateral intakes. With regard to previous laboratory studies, it was shown that submerged plates could change the flow patterns in front of an intake so that the incoming sediments could be reduced by 31% [21]. By applying Flow-3D (version 10.1), Sarhadi and Jabbari [22] confirmed that the parallel arrangement of plates with an angle of 60 degrees does not provide suitable conditions for increasing the relative flow rates in the lateral channel; whereas the plaid and linear arrangement offers the best conditions for transferring the flow to the intake channel. The Flow-3D numerical model simulations by Firozjaei et al. [23] revealed that the circulation area between the submerged plates and the lateral walls of the main channel increases the intake efficiency and reduces the amount of sediments entering the lateral intake. Baltazar et al. [24] found that, in comparison to the case without elements, the plates changed their near-velocity field by creating vortices and increasing the dimensions of the separation zone inside the intake channel. Al-Zubaidy and Ismaeil [10] found that secondary eddies resulting from submerged plates depend on the arrangement of the latter, which causes a change in the velocity distribution patterns and, as a result, reduces sedimentation and sediment entry into the intake channel. Further, the physical modelling of Moghadam et al. [25] revealed that using parallel and staggered submerged vanes at 10- and 30-degree angles would reduce shear stresses at the intake in comparison to the case without vanes.

With regard to the use of spur dikes in order to increase the hydraulic efficiency of lateral intakes, the numerical results of Shamloo et al. [26] showed that the performance of the vanes may be increased using a proper spur dike, thus mitigating the bed-load sediment rate into the intake channel. Analyzing the flow velocity and scour around a T-shaped spur dike in a 90-degree bend, Daneshfaraz et al. [27] noticed that, in the bend without a spur dike, the scour rate was five times higher than in the case with a spur dike. Based on 3D numerical models and laboratory experiments, Karami et al. [28] found that shear stresses increase in the main channel toward the entrance of the diversion channel. Their research considered the presence of spur dikes and vanes. They also found that sedimentation occurs in the vortex areas within the diversion channel and behind the dike in the main channel. The placement of a spur dike perpendicular to the approach flow, upstream of the intake inlet and on the opposite bank with L_S/W_c = 0.2 (where L_S is the spur dike length and W_c is the main channel width), not only reduced the sediment load to the intake channel but also doubled the diverted discharge. Moreover, shear stresses decreased in the main channel due to moving away from the entrance of the diversion channel as a result of the gradual weakening of secondary flows and the reduction in discharge and velocity in the main channel. Geravandi et al. [29] investigated the placement of L-shaped spur dikes upstream and downstream of lateral intakes in an internal river bend. They concluded that the flow velocity at the intake inlet increased. Hence, the best spur dike deflection angle, among the angles of 30, 45, 60, and 90 degrees, was investigated, looking at the maximum

inlet flow rate. The best angle was found to be equal to 60 degrees. Zamani et al. [30] experimentally investigated the effect of a spur dike in increasing the intake discharge and minimizing the turbulence, erosion, and sedimentation. Their results showed that the spur dikes in front of the intake inlet and just downstream of it involved the highest discharge ratio. However, the smallest rate of erosion and sedimentation was achieved when the spur dike was located upstream of the intake channel. Finally, Moradinejad et al. [31] performed an experimental study on the flow patterns and sedimentation at intake structures using spur dikes and skimming walls. They showed that a trench is created towards the intake structure when using a skimming wall, which in turn increases the intake efficiency up to 66% in the case of a skimming wall only and up to 81% when also a spur dike is also placed.

However, the effects of spur dikes on the hydraulic efficiency of side intakes are not clear. This study aims to contribute to this field. The location, effective length, and deviation angle of a spur dike are considered to investigate the hydraulic efficiency of side intakes in terms of water depths, flow velocities, shear stresses, and sedimentation. This is carried out with contextualization to the real case of the Hemmat Water Intake, in Iran. Several numerical simulations were performed by using the Flow-3D (version 11.0.4) Computational Fluid Dynamics (CFD) software in this regard. All the scenarios and simulations were based on the lowest flow rate of 12 m^3/s to focus on simple (but substantially ordinary) conditions.

2. Materials and Methods

2.1. Survey of the Area under Study

The lateral intake of the Shahid Hemmat Dam is located on the Jarahi River in Khuzestan province, upstream of Shadegan City in Iran (Figure 1). This small dam is intended to raise the water level and provide the necessary water depth for the suction pond of the pumping station, which is 28.8 m long on the river. An intake facility with a capacity of 10 m^3/s was built on the right bank of the river to supply the required water to the pumping station. The inlet angle of the intake is 60 degrees with the central axis of the river. During periods of water scarcity (i.e., dry season)—and therefore of low flows of the Jarahi River—the inlet flow depths at the lateral intake are quite low and the water heads at the pumping station are not enough. Moreover, the approaching flow velocities are very low, leading to sedimentation at the entrance and inside the lateral intake. These are the main factors causing low efficiency and sediment accumulation at the Hemmat Water Intake. Hence, finding a solution to these issues and increasing the intake hydraulic efficiency performing numerical simulations of different scenarios is the main aim of this research. The Flow-3D model was employed for these purposes.

The area under study was carefully surveyed. The river characteristics were gathered from 160 m upstream of the dam to 25 m downstream of the dam. Topographical surveys to get all the physical features of the structures were also carried out. The topography map of the station and its upstream and downstream river bed, with a scale of 1:500, was prepared using the direct ground method (Ahadiyan et al. [32]). The studied area was mapped, and a number of points were obtained. Then, the basic information of bed elevation measurements according to the original scale was entered into AutoCAD software, the 3D shape was output, and the same file was defined for Flow-3D. The effective width of the river was B_r = 30 m and the width of the intake inlet was b_{i1} = 21 m. Based on the information from the hydrometric station, the flow depths of 1.35, 2.20, 2.80, 3.70, and 4.38 m were identified for the flow rates of 12, 32, 62, 100, and 143 m^3/s, respectively (Ahadiyan et al. [32]). Topographic and bathymetric data can be made available upon direct request to the authors of the present paper. Table 1 provides some key physical features as well as some target parameters, such as the spur dike length and position. As previously reported, the parameters which have been considered include: (i) three alternative locations of the spur dike (i.e., a spur dike placed on the opposite side of the intake inlet and aligned with the upstream edge of the intake inlet, to be regarded as a witness spur dike; a spur dike placed at a distance D_S of 7 m downstream of the witness spur dike placement, which implies a dimensionless distance D_S/b_{i1} of 1/3, with b_{i1} being

the intake opening width; and a spur dike at a distance of 7 m upstream of the witness spur dike placement with a dimensionless distance, still, of 1/3); (ii) four relative spur dike lengths, L_S/B_r, of 0.24, 0.32, 0.40, and 0.46, with L_S being the effective spur dike length and B_r the approaching river width; and (iii) five spur dike deviation angles of 75, 90, 105, 120, and 135 degrees. All these configurations, almost equally spaced between them, would cover all possible arrangements of a spur dike at the Hemmat Water Intake. Further configurations outside the ranges here considered would be ineffective or impracticable. Figure 2 shows a 3D view of the area under study as introduced in the Flow-3D model.

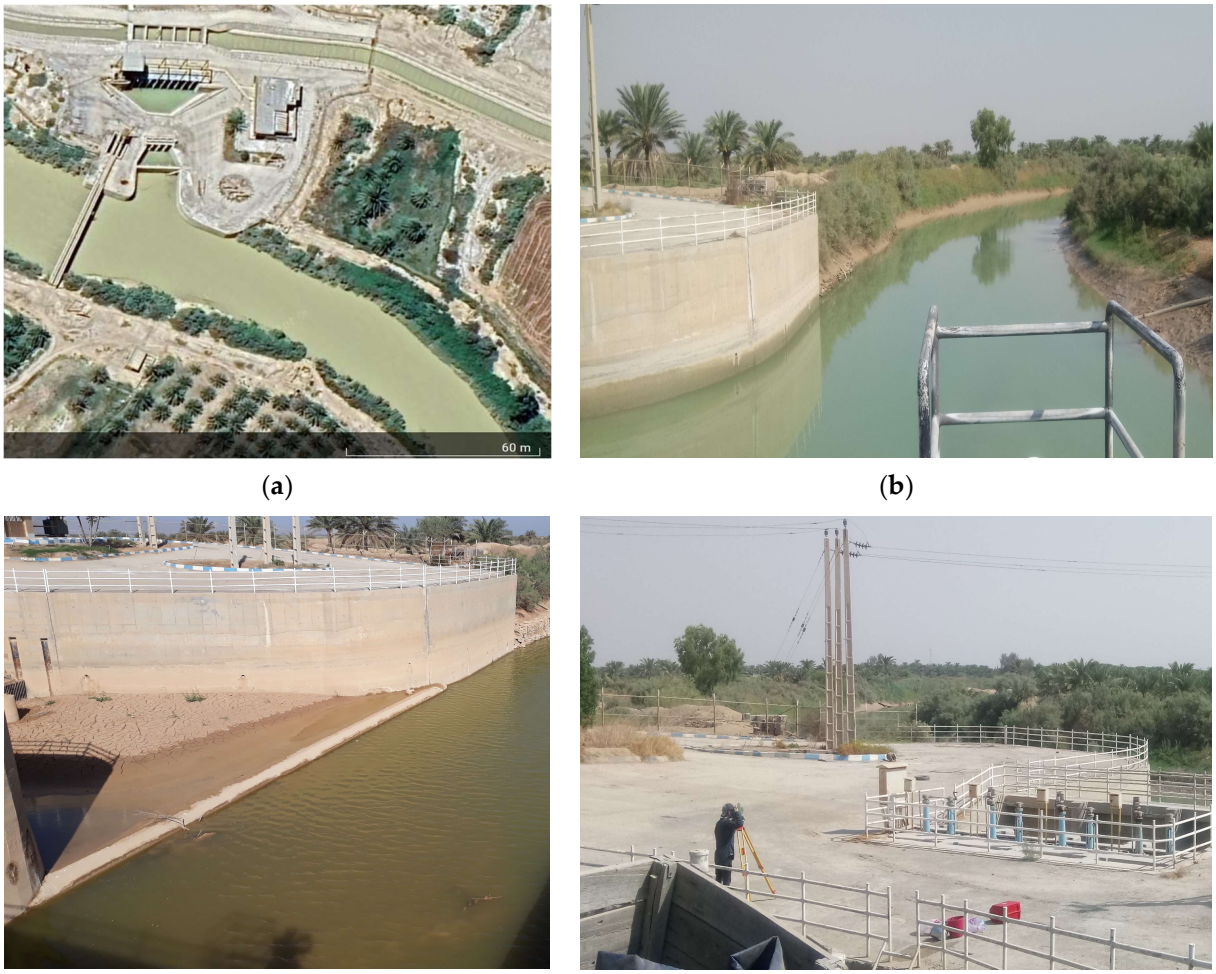


Figure 1. Photographs of the lateral intake structure of the Shahid Hemmat Dam. (**a**) Aerial view of the Hemmat Dam, lateral intake, and pumping station; (**b**) intake inlet from the top of the pumping station; (**c**) sedimentation at the intake inlet; (**d**) pumping station.

Table 1. Some physical features of the area under study and target parameters for spur dikes.

Distance of the Spur Dike Base from the Witness Spur Dike D_S [m]	Effective Spur Dike Length L_S [m]	Intake Inlet Width b_{i1} [m]	Effective River Width B_r [m]
7	7.2, 9.6, 12, 14	21	30

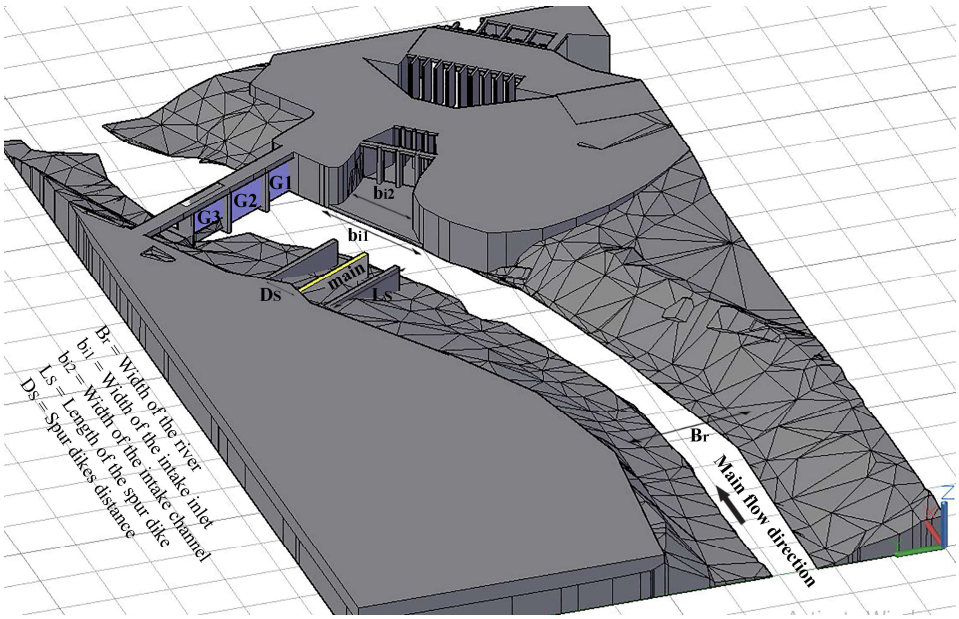


Figure 2. 3D view of the monitored area (and structures) and target parameters used in simulations. B_r: main river width; b_i1: intake inlet width; b_i2: intake channel width; L_S: spur dike length, D_S: distance of the spur dike base from the witness spur dike; G1, G2, and G3: dam gates.

2.2. Numerical Simulations

2.2.1. Notes on Flow-3D Model and Its Implementation

Flow-3D is a well-known and established computational fluid dynamics program. The model uses the volume of fluid (VOF) method on a gridded domain to solve the Navier–Stokes–Reynolds equations for three-dimensional analysis of incompressible flows. Flow-3D uses an advanced free surface flow tracking algorithm (TruVOF) developed by Hirt and Nichols [33], in which fluid configurations are defined in terms of a VOF function $F(x,y,z,t)$. Cells are represented by a cell-fill variable (i.e., fraction function) value representing the ratio of the fluid volume to the cell volume; the empty cells have a value of zero, whole cells a value of one, and cells that contain the free surface a value in the range 0–1. The water surface is then tracked in space and time as a first-order approximation according to the fluid-to-cell volume ratio and the location of the fluid in the surrounding cells. The TruVOF method considers only the fluid's value, not the air's; gas cells are considered empty. Previous studies used this method to reduce the time cost and graphically describe the free surface shape [34–36]. Considering that the main concern of this research is to increase the water diversion efficiency of the Hemmat Water Intake when the river has the lowest inflow, an initial flow of 12 m^3/s was considered in all the implementations and simulations, according to the actual conditions. The spur dike was alternatively located in three different places along the bank, in front of the intake inlet with a distance D_S of 7 m in comparison with the witness spur dike. This implies a relative distance D_S/b_{i1} equal to 1/3. The reason for choosing this distance is that placing a spur dike at a relative distance greater than 1/3 would either not conveniently address the flow towards the intake inlet or require a spur dike too close to the dam. As mentioned above, four spur dike lengths L_S were selected for this study, with values of the ratio L_S/B_r, respectively, equal to 24%, 32%, 40%, and 46%. Moreover, the following spur dike deviation angles were investigated: 75, 90, 105, 120, and 135 degrees. As mentioned earlier, the deviation angle is defined as the angle between the spur dike axis and the original river-bank line from which the spur dike extends. A spur dike pointing downstream has a deviation angle greater than 90 degrees.

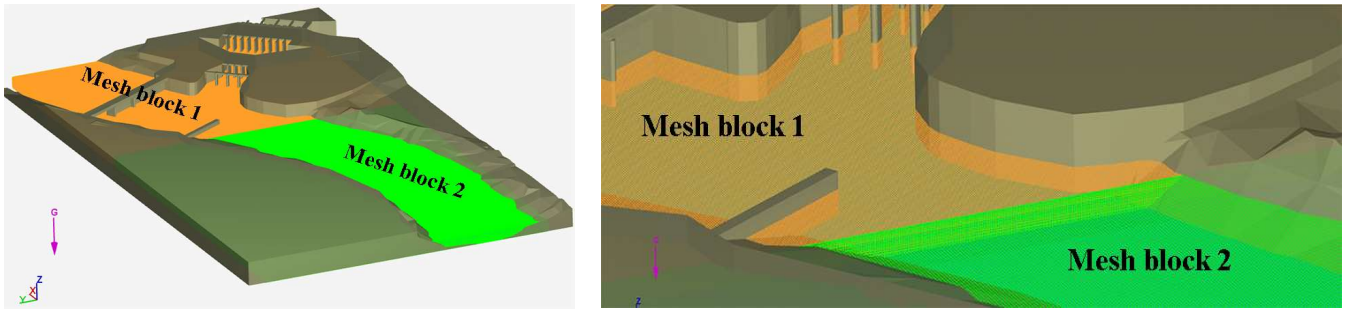
2.2.2. Meshing and Boundary Conditions

The simulations were performed for different scenarios (Table 2) to investigate the effect of the spur dike location, length, and angle on the hydraulic efficiency of the lateral intake.

Table 2. Geometric conditions for the scenarios investigated in this study. D_S/b_{i1} is the ratio of the distance D_S between the base of the spur dike and the witness spur dike (i.e., S main) to the intake inlet width b_{i1}; L_S/B_r is the ratio of the spur dike effective length L_S to the river width B_r; and θ is the spur dike deflection angle.

Scenario	D_S/b_{i1}	L_S/B_r	θ (Degrees)
1	S main	0.24	90
2	S main	0.32	90
3	S main	0.40	90
4	S main	0.46	90
5	−1/3	0.32	90
6	+1/3	0.32	90
7	S main	0.32	75
8	S main	0.32	105
9	S main	0.32	120
10	S main	0.32	135
11	S main (all gates open)	0.32	90
12	No spur dike (all gates open)	-	-
13	No spur dike (3rd gate open)	-	-

The time duration for each run was considered to be 120 s after a trial-and-error analysis. Meshing around the spur dike and the intake structure included two parts: a first part from upstream of the spur dike to the outlet border (Mesh block 1) with smaller mesh elements including 2,804,660 cells; a second part from (nearly) the upstream face of the spur dike to the river approach section (Mesh block 2) with larger mesh elements including 1,000,000 cells. As the flow entered the next mesh block without changing, the boundary conditions between these two parts of the mesh cube were considered symmetric. Figure 3 shows two views of the meshing blocks.



(**a**) (**b**)

Figure 3. Meshing around the intake structure and spur dike. (**a**) General view of the two mesh blocks; (**b**) magnification of the two mesh blocks around the intake inlet and the spur dike.

In each test, the number of mesh cells was determined and executed after investigating different meshes to find the optimal mesh.

The more mesh cells there were, the smaller their size as well as the more complete and the more accurate were the details, such as those for the spur dike and the entrance edge of the intake structure introduced to the software. Where the size of mesh cells was larger, or their amount was smaller, the edge of the spur dike was not well-introduced to the software. Table 3 presents some tests performed until the optimal mesh was found.

Table 3. Details of some tests to find the optimal mesh. The aspect ratio is the ratio of a cell's longest length to the shortest length. The ideal aspect ratio would be 1. X, Y, and Z directions are defined in Figure 2.

Mesh	1	2	3	4
Total number of real cells	1,348,763	3,445,038	1,975,560	2,804,660
Number of real cells (X direction)	289	393	326	365
Number of real cells (Y direction)	359	487	404	452
Number of real cells (Z direction)	13	18	15	17
Maximum aspect ratios (X-Y direction)	1.001	1.000	1.000	1.001
Maximum aspect ratios (Y-Z direction)	1.036	1.015	1.010	1.002
Maximum aspect ratios (Z-X direction)	1.034	1.016	1.011	1.000

The number of mesh cells was determined separately in each X, Y, and Z direction. According to Table 3, the maximum aspect ratio values were slightly higher than 1, which is a perfect value without errors. Finally, the optimal number of mesh cells (Mesh No. 4) without errors with a good finish of all parts of the structures was achieved. The optimal mesh had a maximum aspect ratio of around 1 for 2,804,660 mesh cells in all three directions. Then, the RNG turbulence model was applied, as recommended by Karami et al. [28] and Babagoli Sefidkoohi et al. [14]. The boundary conditions were an inflow discharge of 12 m^3/s for the river, two outflows including the lateral intake and the river reach downstream of the intake structure, and fixed riverbanks. Then, the border on both sides and the bottom of the river were considered as a wall (impermeable contours). The downstream boundary condition of the river was defined as outflow. Numerical simulations were carried out under clear-water conditions by considering the equivalent roughness of bed sediments. The bed roughness was calculated based on the particle size to apply the effect of the river bed on the flow velocity. Figure 4 and Table 4 provide some information on the numerical boundary conditions. Calibration was also done by comparing flow velocity and depth outputs to the measured data.

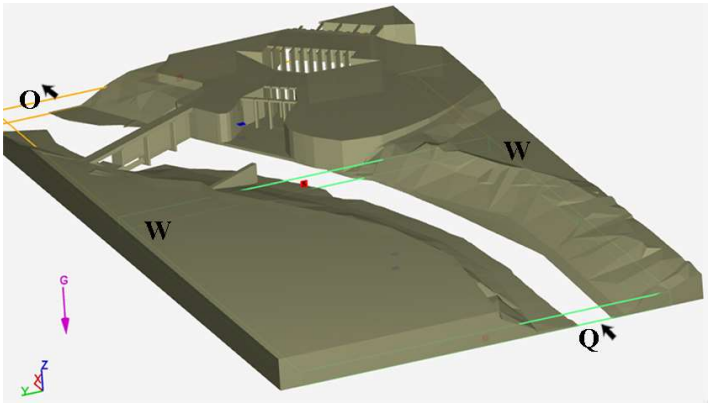


Figure 4. Overview on the upstream (Q), downstream (O), and lateral (W) boundary conditions.

Table 4. Details on the upstream, downstream, and lateral boundary conditions considered in this study.

Boundaries	Boundary Conditions
X Min	VFR (Volume Flow Rate)
X Max	O (Outflow)
Y Min	W (Wall)
Y Max	W (Wall)
Z Min	W (Wall)
Z Max	S (Symmetry)

Finally, in regard to the shear stresses distribution on the river bed, the following equations have been considered, according to Knight et al. [37]:

$$\begin{aligned} \tau_{bx} &= \frac{\rho g}{c^2}\overline{u}\sqrt{\overline{u}^2+\overline{v}^2} \\ \tau_{by} &= \frac{\rho g}{c^2}\overline{v}\sqrt{\overline{u}^2+\overline{v}^2} \\ \tau_b &= \sqrt{(\tau_{bx}^2+\tau_{by}^2)} \end{aligned} \quad (1)$$

where τ_{bx}, τ_{by}, and τ_b are the bed shear stresses in the longitudinal and transverse directions and the total shear stress, respectively. Also, $\overline{u}$ and $\overline{v}$ are the average velocities in the longitudinal and transverse directions at each section. Moreover, g, ρ, and c are the acceleration of gravity, the fluid density, and the Chézy coefficient, respectively.

2.2.3. Calibration of Flow-3D Model

The calibration of the Flow-3D model was done for the real flow of 12 m^3/s according to the velocity data at three points with distances of 100, 85, and 70 m upstream of the dam and in the central line of the river (Ahadiyan et al. [32]). The field data were compared with the numerical results for four distinct opening configurations of the gates. Namely, configuration#1 in which only gate No. 1 was open, configuration#2 in which only gate No. 2 was open, configuration#3 in which only gate No. 3 was open, and configuration#4 in which all gates were open. Ahadiyan et al. [32] showed a suitable agreement between the real and numerical data, with errors between 3.3% and 8.6%.

3. Results and Discussion

Several scenarios were investigated, including those aimed at increasing the efficiency of the Hemmat Water Intake and reducing the sediment deposition in conditions of water scarcity during dry seasons. Therefore, several simulations have been performed to detect the optimal configurations in terms of the best allocation, length, and deviation angle for a spur dike along the front of the intake inlet. Hence, different scenarios were analyzed through field investigation and numerical modelling.

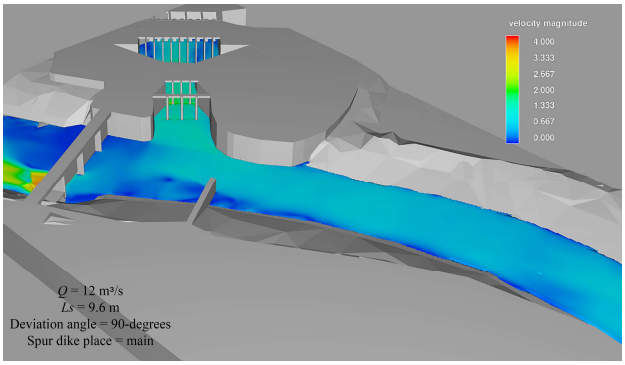
In general, some considerations might be anticipated: (i) A spur dike causes a contraction of the flow path and, as a result, an increase in the flow velocity in the surroundings of its end and an increase in the average velocity in the contracted section. For a given river width and approaching flow discharge, these flow velocity amplifications become larger by increasing amounts as the spur dike length increases. Therefore, it is expected that the placement of a spur dike on the opposite side of a lateral intake would increase the flow velocities at the intake inlet as well as the shear stresses, thus reducing the sedimentation phenomena. The placement of the spur dike in comparison to the intake inlet would impact the position of the contracted flow region. It is understandable that, when the spur dike is aligned with the upstream edge of the intake inlet, the contracted flow region will most likely tend to extend along the entire intake inlet. Conversely, the placement of the spur dike upstream or downstream of the upstream edge of the intake inlet would only lead to partial overlapping between the contracted flow region and the intake inlet area. (ii) At a given river width and approaching discharge, the deviation angle for spur dikes pointing downstream would reduce the contracted flow region as the deviation angle increases. However, for deviation angles greater than 90 degrees (i.e., attracting spur dike), the scouring phenomena are less intense in comparison to a spur dike with a deviation angle of 90 degrees (i.e., deflecting spur dike) or deviation angle less than 90 degrees (i.e., repelling spur dike). Therefore, although an attracting spur dike would (slightly) reduce flow depths and flow velocities, scouring phenomena are alleviated and the spur dike stability is better preserved.

More specifically, in this study, when the effect of the gates is considered, the condition of only gate No. 3 being open is focused on. Indeed, gate No. 3 would determine the

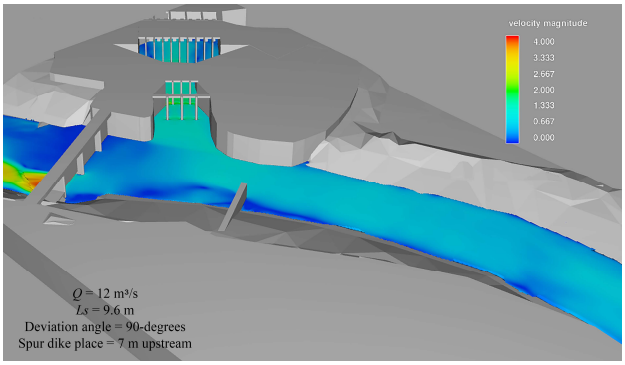
most critical state in terms of the minimum diverted discharge through the intake inlet due to its distance from the pumping station (greater than that of the other two gates). Moreover, in the case that the gates are open, the effect and efficiency of the spur dike become more meaningful and clearer when only gate No. 3 is open. Opening the other two gates would make the effect of the spur dike less discernible. The results focusing on different arrangements of open and closed gates, with the spur dike or not, can be found in Ahadiyan et al. [32]. Moreover, it may be important to highlight that, in the following analyses, the sedimentation processes are only presumed to be closely connected with the kinematic fields and/or shear stresses.

3.1. Changes in Flow Patterns at the Intake Inlet as the Position of the Spur Dike Changes

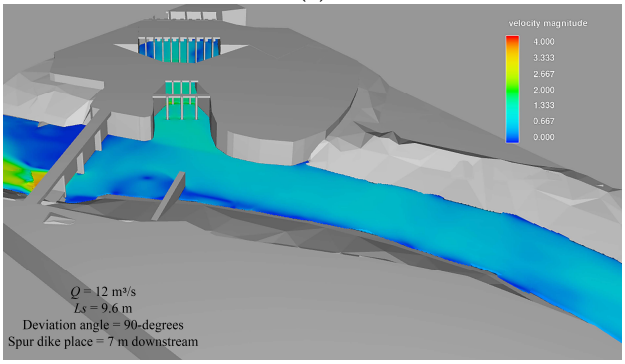
Figure 5 shows the flow pattern variations at the intake inlet affected by the spur dike position for steady flow and in the case of gate No. 3 being open. The spur dike is perpendicular to the approach flow and its alternative placements are: in front of the upstream edge of the intake structure with the base in the opposite bank (witness spur dike, Figure 5a, scenario 2), −7 m upstream of the position of the witness spur dike (Figure 5b, scenario 5), and +7 m downstream of the position of the witness spur dike (Figure 5c, scenario 6). The models were run with the river base discharge during a water shortage scenario and considering the three locations for the spur dike. However, the results on the kinematic fields were similar. Hence, the flow velocities around the intake structure and the spur dike did not change much in these three positions.



(**a**)



(**b**)



(**c**)

Figure 5. Flow velocity distribution around the dam, intake structure, and spur dike for the following positions of the latter: (**a**) in front of the upstream edge of the intake structure (witness spur dike); (**b**) 7 m upstream of the position of the witness spur dike; (**c**) 7 m downstream of the position of the witness spur dike. In the legend, flow velocities are in m/s and range from 0.0 to 4.0 m/s with steps of 0.667 m/s.

For example, the average flow velocity in the river (100 m upstream of the dam at the river centerline) was 1.5 m/s (V/V_{max} = 0.94, with V_{max} = maximum flow velocity in all runs) at the intake inlet (point 2 in Figure 6) for the witness spur dike. Meanwhile, in the

case of the other positions of the spur dike on the upstream and downstream regions, this value reached 1.47 and 1.48 m/s (V/V_{max} = 0.93), respectively. In all three displacement modes, and especially in the case of the witness spur dike (Figure 5a), a large part of the main flow was directed toward the intake inlet due to the presence of the spur dike and its influential role in directing the flow.

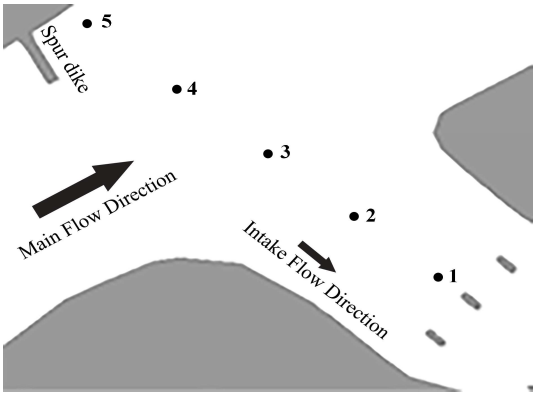


Figure 6. Position of the five control points for local velocity comparisons.

Figure 6 shows the position of the five control points for comparison of the local velocities for the different scenarios.

Figure 7 shows the average flow velocities from the centerline of the intake channel to the opposite riverbank (point 5), with an initial flow rate of 12 m^3/s, gate No. 3 being open, and three different positions of the spur dike. The results show that the flow velocities were very close at points 1, 2, and 3 for all three spur dike locations. On the other hand, a flow velocity gradient occurs at points 1 and 2, in comparison to the other points, due to the more significant impact of the spur dike on this area and their close proximity to the intake inlet. However, the local velocities at points 4 and 5 for $D_S/b_{i1} = -1/3$ are 0.55 m/s (V/V_{max} = 0.34) and 0.47 m/s (V/V_{max} = 0.29), respectively. Meanwhile, in the case of $D_S/b_{i1} = +1/3$, they were 0.29 m/s (V/V_{max} = 0.18) and 0.10 m/s (V/V_{max} = 0.06). The reasons for these discrepancies are the changes in the velocity gradient due to the spur dike base being oriented into the river flow, which causes the development of low-velocity areas and eddies. These low-velocity areas were also transferred (as shown in Figure 5) by changing the location of the spur dike, but they did not affect the average flow velocities entering the intake channel (i.e., points 1 and 2).

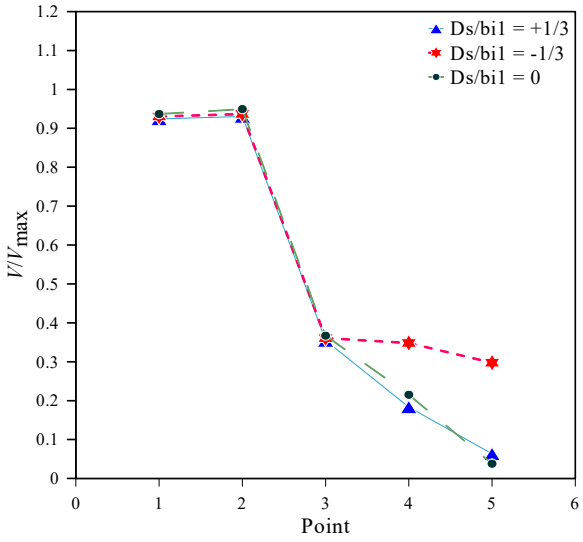


Figure 7. Flow velocities along the transect shown in Figure 6 for different positions of the spur dike.

According to Figures 8–10, four main vortices are formed by comparing the streamlines in the three positions of the spur dikes. They include: the small eddy upstream of the spur dike (Vortex 1) that is formed under the riverside shelter near the structure and is known as the primary eddy or horseshoe vortex; the larger eddy downstream of the spur dike (Vortex 2) that is known as the updraft eddy [38–40]; and two eddies in the intake basin (Vortex 3 and Vortex 4). The power of these eddies decreases or increases when changing the spur dike position. Vortex 1 becomes more powerful when the spur dike positions are downstream or upstream of the main spur dike (Figures 8–10). Meanwhile, this vortex becomes weaker in the case of the witness spur dike being located in front of the upstream edge of the intake inlet (Figure 9). Vortex 2 has an opposite behaviour. This vortex becomes smaller and weaker when moving the spur dike downstream or upstream with respect to the position of the witness spur dike (Figures 8 and 10 under scenarios 5 and 6, respectively, compared to Figure 9 with scenario 2). Moreover, Vortex 2 has larger dimensions and is more power compared to the other vortices, especially when the spur dike is positioned downstream of the main spur dike (Figure 8 with scenario 5). Interestingly, this result is consistent with those obtained by Koken and Constantinescu [41].

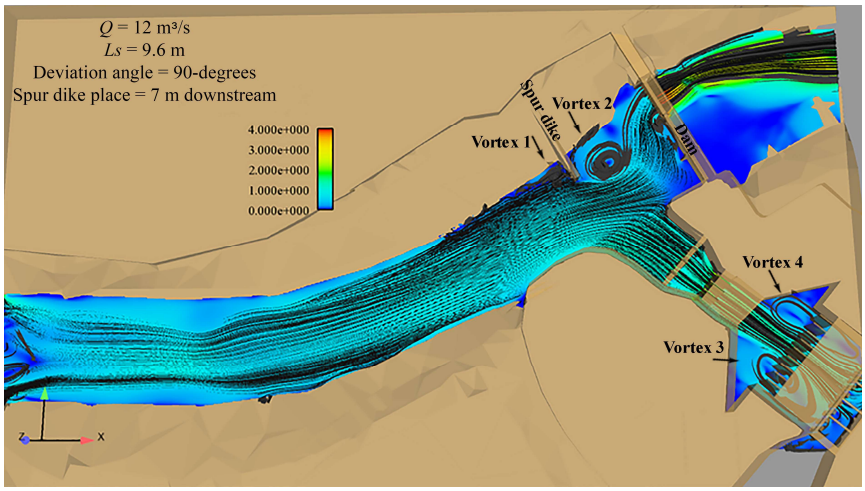


Figure 8. Simulation of the vortices at and around the intake structure in the case of a spur dike placed downstream of the witness spur dike. In the legend, flow velocities are in m/s and range from 0.0 to 4.0 m/s with steps of 1.0 m/s.

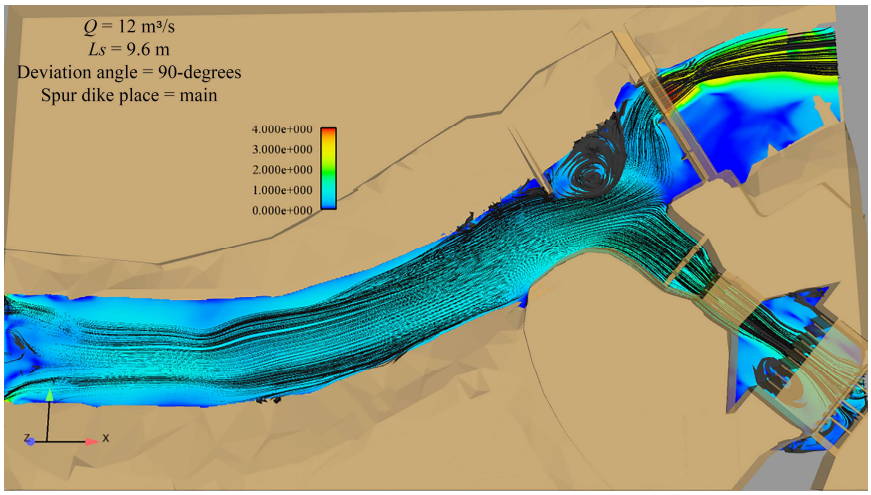


Figure 9. Simulation of the vortices at and around the intake structure in the case of the witness spur dike. In the legend, flow velocities are in m/s and range from 0.0 to 4.0 m/s with steps of 1.0 m/s.

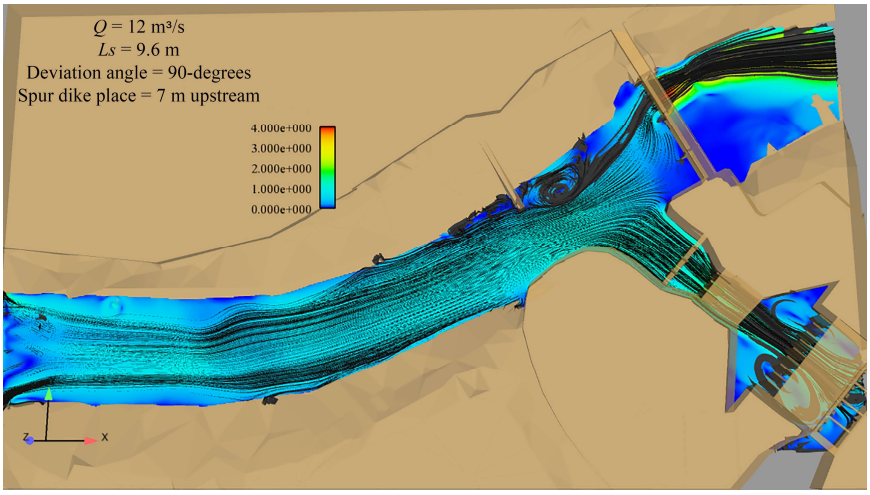


Figure 10. Simulation of the vortices at and around the intake structure in the case of a spur dike placed upstream of the witness spur dike. In the legend, flow velocities are in m/s and range from 0.0 to 4.0 m/s with steps of 1.0 m/s.

3.2. Changes in Flow Patterns at the Intake Inlet as the Length of the Spur Dike Changes

Figure 11a–d shows the effects of the spur dike length on the characteristics of the flow around the intake inlet (scenarios 1–4). The length of the spur dike was either 7.2, 9.6, 12, or 14 m. The spur dike was on the opposite side of the intake inlet, aligned with the upstream edge of the intake inlet (i.e., witness spur dike) and perpendicular to the original riverbank (90 degrees). Only gate No. 3 was open. It was found that the flow velocity at the intake inlet was directly related to the spur dike length. As the length of the spur dike increased, the river flow was better directed towards the intake structure, with an increase in discharge and flow velocity. The results in terms of flow velocity in Figure 12 show that the maximum spur dike length (L_S/B_r = 0.46, scenario 4) compared to the minimum spur dike length (L_S/B_r = 0.24, scenario 1) caused an increase of 11% for the inflow velocity at the intake inlet. As mentioned above, L_S is the spur dike length and B_r is the river width. Specifically, for an L_S equal to 14 m, the velocity was 1.58 m/s (V/V_{max} = 1.00) while, for an L_S equal to 7.2 m, the velocity was 1.42 m/s (V/V_{max} = 0.89). The effect of the spur dike length on the generation of eddies is stronger the longer the spur dike length is. There is no formation of vortices for the shorter spur dike with L_S/B_r = 0.24. In this case, the flow is uniformly directed toward gate No. 3.

Figure 12 compares the effects of the spur dike length on the flow velocities at the five points previously considered in Figure 6. The results show that the highest flow velocities in all cases are found at points 1 and 2, near the entrance of the intake channel. The highest flow velocities are found for the spur dike with an L_S/B_r = 0.46 (scenario 4) and the maximum value is found at point 2. At this point, the velocity is 1.58 m/s (V/V_{max} = 1.00) while, for L_S/B_r = 0.24 (scenario 1), the velocity is equal to 1.42 m/s (V/V_{max} = 0.89), which shows an increase of 11% when passing from the shortest spur dike to the longest one. The greatest change in flow velocities occurs at point 3, with a drastic decrease when moving from the longer to the shorter spur dike. Specifically, the average velocity at point 3 for the spur dike with an L_S/B_r = 0.24 is 0.52 m/s (V/V_{max} = 0.33), while at the same point the velocity is 1.55 m/s (V/V_{max} = 0.98) with an increase of 198% when the L_S/B_r = 0.46. This is due to the fact that point 3 is placed in a high-velocity area around the nose of the longest spur dike.

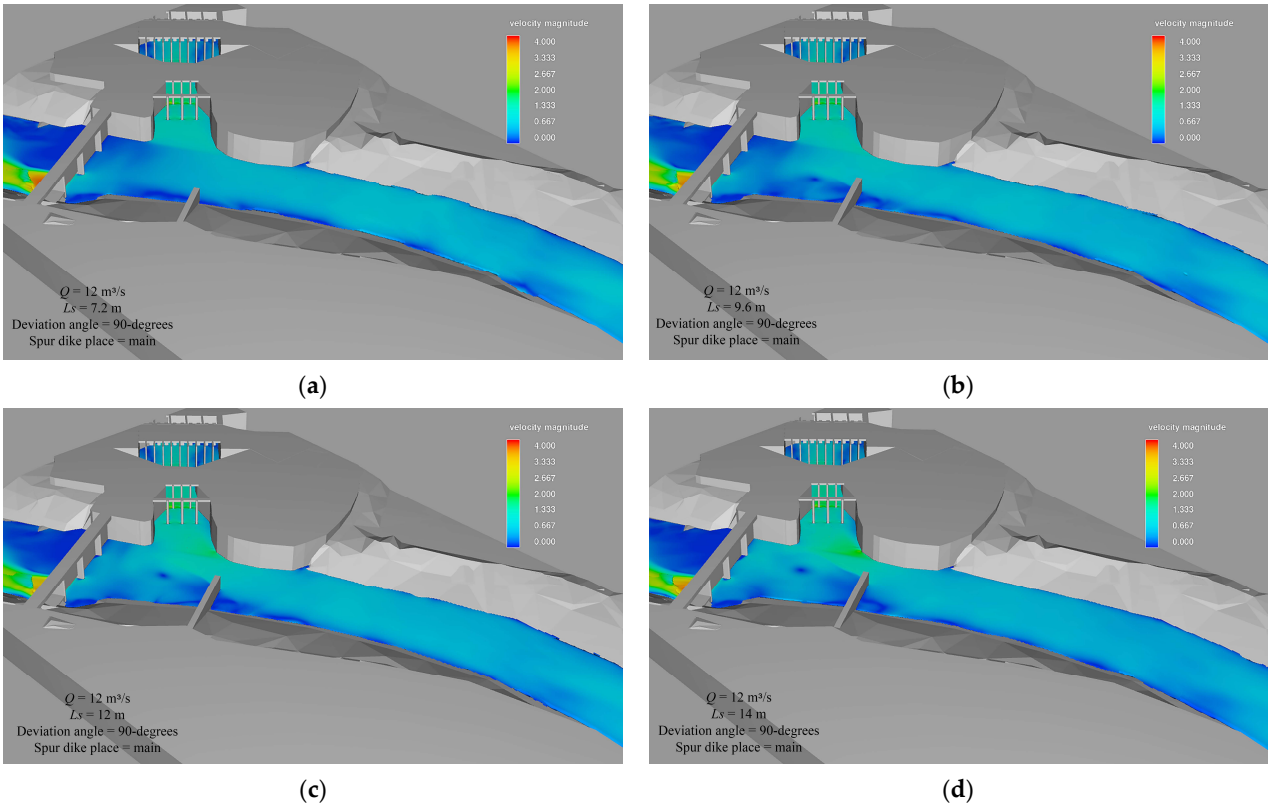


Figure 11. Simulation of the kinematic field around the intake inlet in the case of a spur dike with: (**a**) L_S/B_r = 0.24; (**b**) L_S/B_r = 0.32; (**c**) L_S/B_r = 0.40; and (**d**) L_S/B_r = 0.46. The approach discharge Q is equal to 12 m^3/s and velocities are given in m/s. In the legend, flow velocities are in m/s and range from 0.0 to 4.0 m/s with steps of 0.667 m/s.

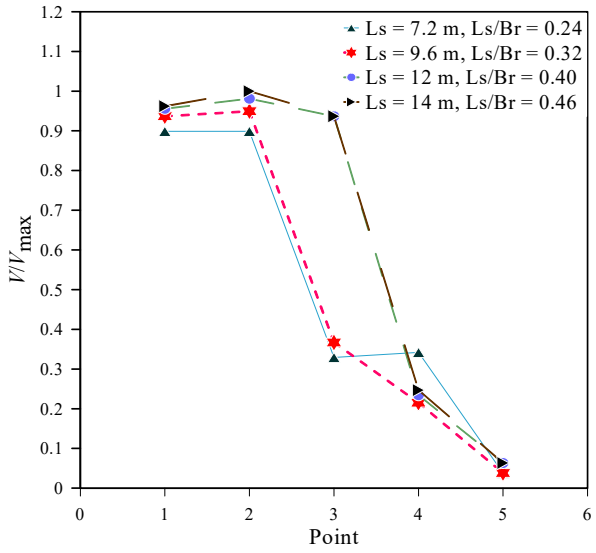


Figure 12. Flow velocities along the transect shown in Figure 6 for different lengths of the spur dike.

3.3. Changes in Flow Patterns at the Intake Inlet as the Deflection Angle of the Spur Dike Changes

Figure 13a–e shows the effects of the spur dike deflection angle on the flow patterns and characteristics around the intake inlet. Five deflection angles were considered, namely 75, 90, 105, 120, and 135 degrees, to which corresponded the scenarios 7, 2, 8, 9, and 10, respectively. As previously said, in this study, the deviation angle is defined as the angle between the spur dike axis and the original riverbank line from which the spur dike extends.

A spur dike pointing downstream has a deviation angle greater than 90 degrees, by way of example. The spur dike length was kept constant such that the L_S/B_r = 0.32. The numerical simulations revealed that no appreciable differences were noted in the kinematic field as the deflection angle varied.

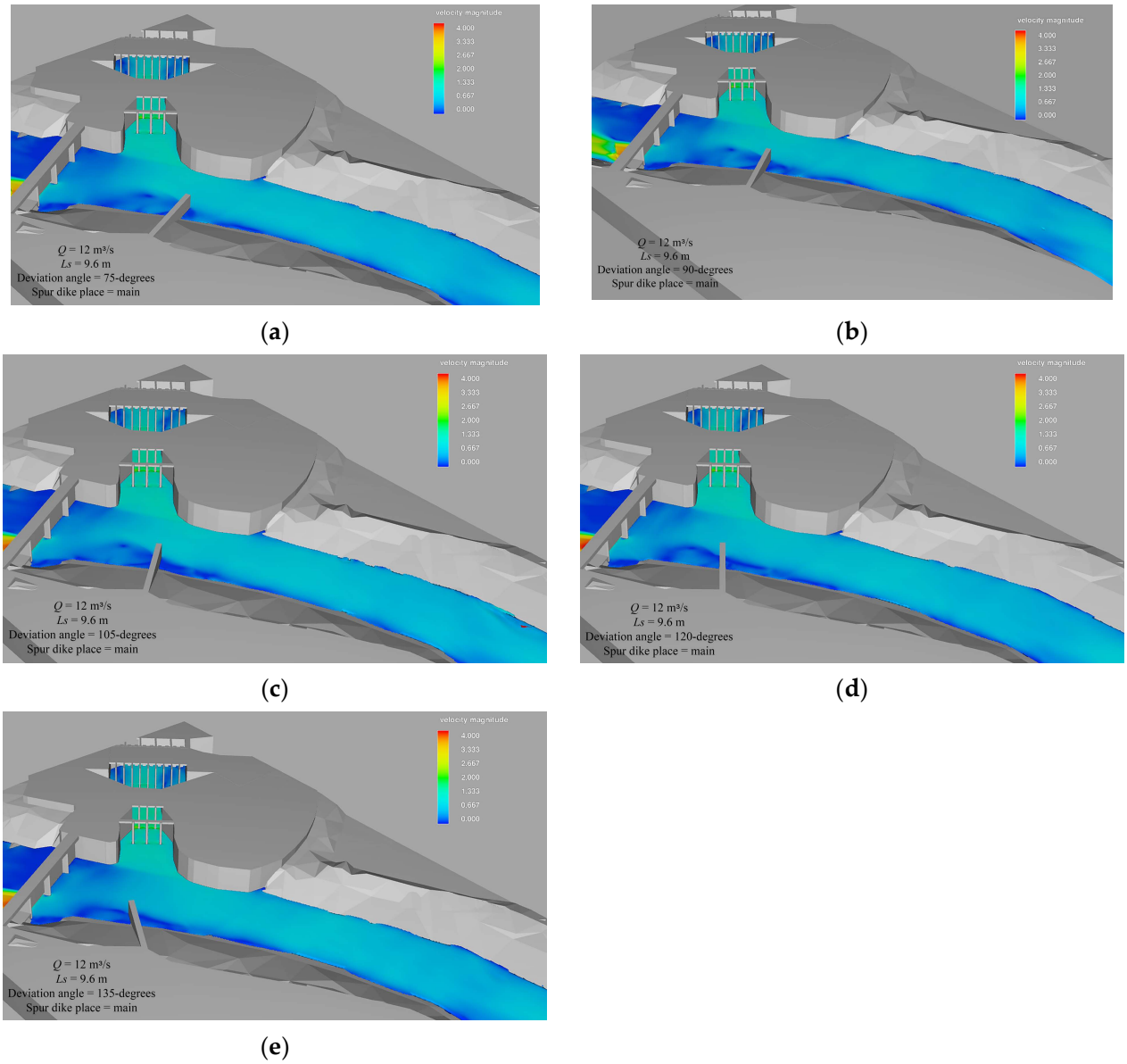


Figure 13. Simulation of the kinematic field around the intake inlet in the case of a spur dike with deflection angle of: (**a**) 75; (**b**) 90; (**c**) 105; (**d**) 120; and (**e**) 135 degrees. The approach discharge Q is equal to 12 m^3/s. In the legend, flow velocities are in m/s and range from 0.0 to 4.0 m/s with steps of 0.667 m/s.

Figure 14 compares the effects of the spur dike deflection angle on the flow velocities at the five points previously considered in Figure 6. It was found that no significant differences in the velocities occurred, especially at points 1 and 2 where the differences were less than 2%. This would imply that the flow velocities at the intake inlet are not much influenced by variations in the deflection angle between 75 and 135 degrees.

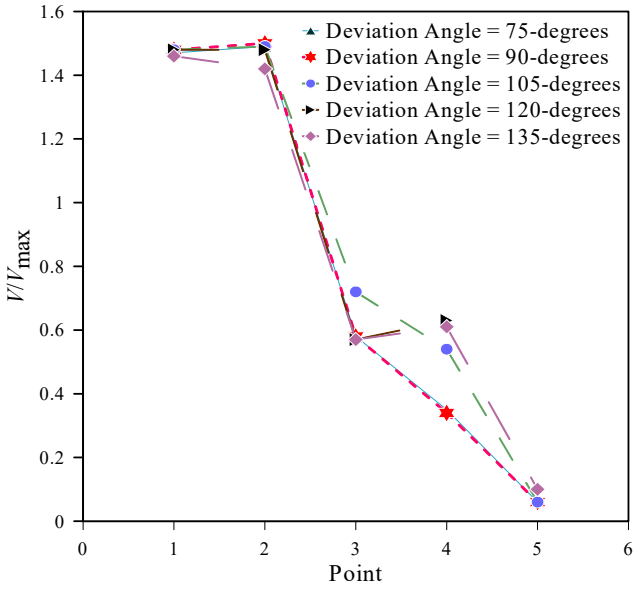


Figure 14. Flow velocities along the transect shown in Figure 6 for different deflection angles of the spur dike.

It should be noted that the deflection angle did not even affect the flow depths. The effects of changes in the spur dike deflection angle on the flow depth, with reference to 12 points along the transect (Figure 15), are shown in Figure 16. The results show that, for a spur dike deviation angle of 135 degrees, the flow depths at the intake inlet are the highest in comparison to the other configurations with different deviation angles. Specifically, the flow depth at the intake inlet increases by about 9% for the spur dike with a deflection angle of 135 degrees in comparison to the one with an angle of 75 degrees. In summary, the results showed that the flow depths increased, albeit in a limited way, with the spur dike deviation angle (from 75 to 135 degrees). Moreover, for all the deviation angles, the highest flow depths occurred at points 5, 6, 7, and 8 with a maximum value of the ratio Z/Z_{max} of about 0.35. Here, Z is the flow depth value and Z_{max} is the maximum flow depth value.

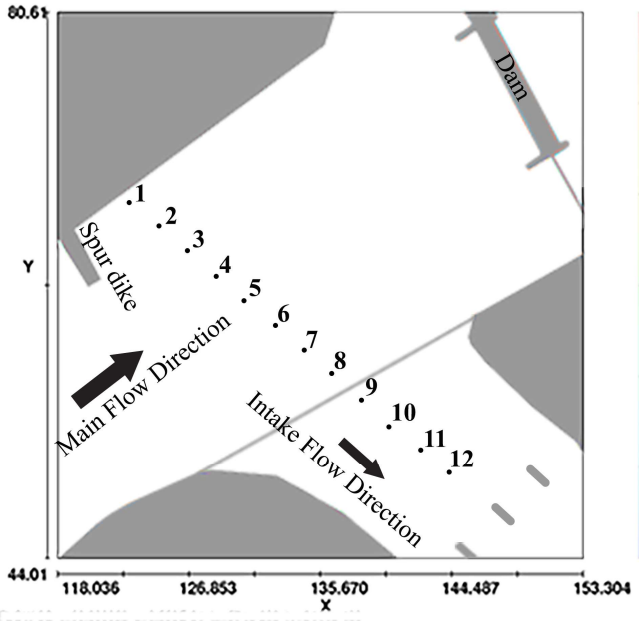


Figure 15. Position of the 12 control points for local flow depth comparisons.

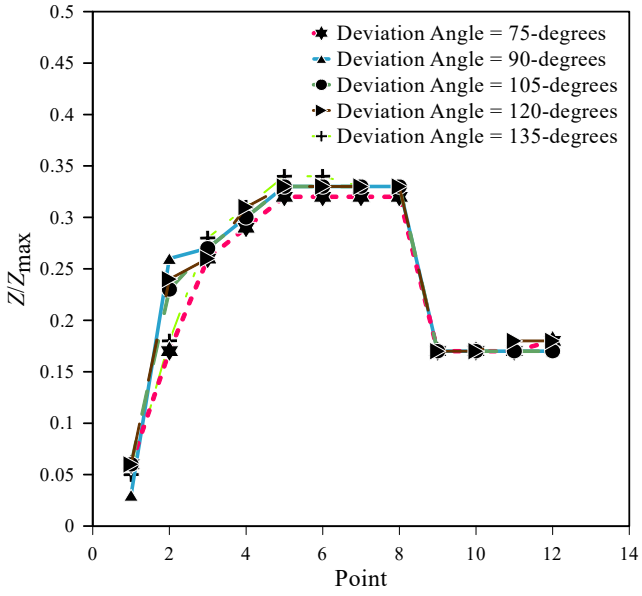


Figure 16. Flow depths *Z* along the transect shown in Figure 15 for different deflection angles of the spur dike. Only gate No. 3 is open and the witness spur dike is placed.

3.4. Bed Shear Stresses Comparison for Different Scenarios

Figure 17 shows three transects with control points for the comparison of shear stresses.

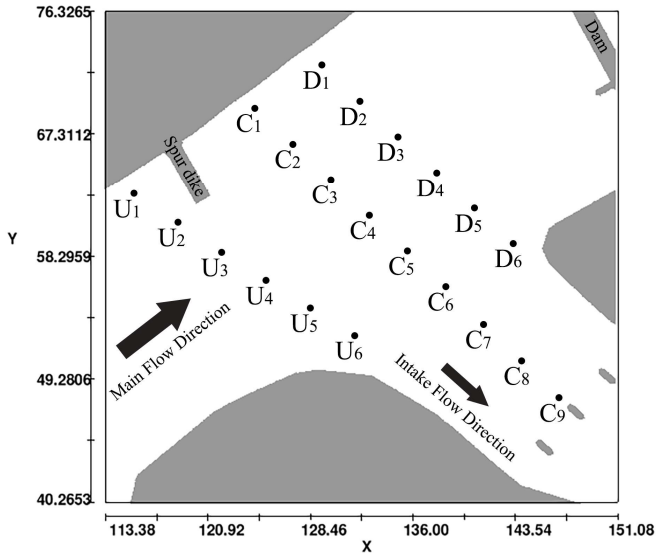


Figure 17. Indication of the three transects with the related control point positions for the comparison of shear stresses for different scenarios.

In Figures 18–20, the bed shear stresses along three transects, including the transect along the intake channel centerline including the points from C1 to C9, the transect upstream of the central one including the points from U1 to U6, and the transect downstream of the central one including the points from D1 to D6, are shown. The central transect with point C extends from the intake channel (along the channel centerline) until nearly the spur dike sidewall. Due to the steepness of the river sidewall and the entrance ramp of the intake channel, some points are located in the solid part of the structure (i.e., points C1, C7, C8, and C9), and thus have no value.

According to Figure 18, the results show that the highest values of the shear stresses, with significant differences from the other cases, occur when the spur dike is used and

when all gates or gate No. 3 only are open. Moreover, the highest values of the shear stresses are related to the points C5, C4, and C3 regardless of the scenario because these points are located in the main river flow. For example, in the case of point C5 without a spur dike and when all gates are open, the shear stress τ_b is equal to 2.28 kPa. Similarly, τ_b is equal to 3.01 kPa when gate No. 3 only is open. Hence, the single opening of gate No. 3 increases the shear stress at point C5 (close to the intake inlet) by 32% in comparison to the configuration in which all gates are open. In this way, the main flow is more strongly diverted towards the intake channel. Therefore, opening gate No. 3 would reduce the possibility of sedimentation in comparison to the opening of all the gates.

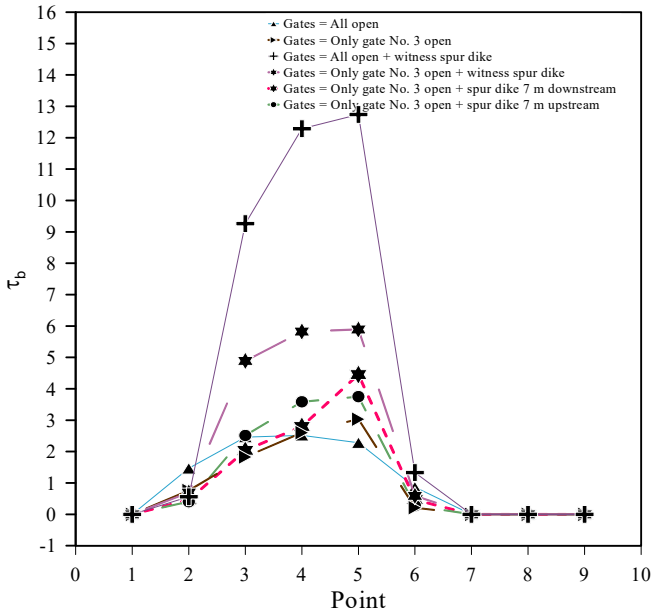


Figure 18. Shear stresses τ_b along the central transect shown in Figure 17. The values are in kPa.

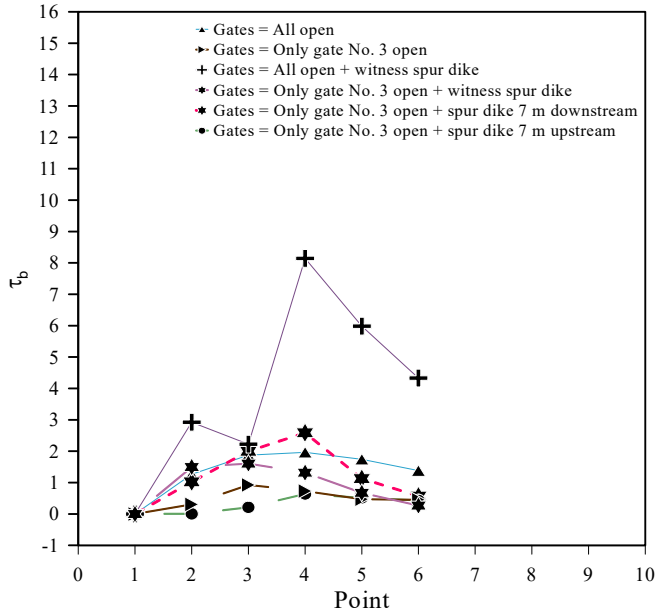


Figure 19. Shear stresses along the transect downstream of the central one shown in Figure 17. The values are in kPa.

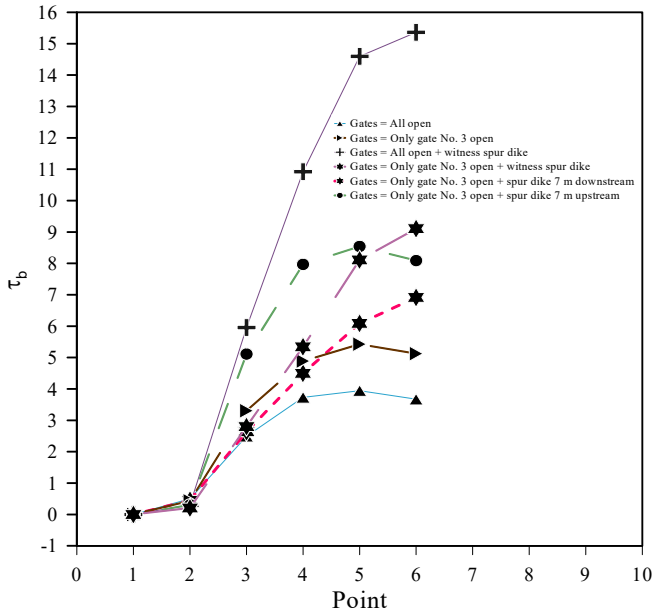


Figure 20. Shear stresses along the transect upstream of the central one shown in Figure 17. The values are in kPa.

On the other hand, the shear stress at point C5 increases up to 12.63 kPa when a spur dike is placed. Then, the shear stress increases more than five times in comparison to the case of the absence of a spur dike when the shear stress is equal to 2.28 kPa. Moreover, looking at point C6 (even closer to the intake inlet) in the case of the presence of a spur dike, the shear stress is equal to 1.31 kPa with an increase of 50% in comparison to the case without a spur dike, in which the shear stress value drops to 0.87 kPa. Hence, the spur dike would increase the flow strength at the intake inlet. Likewise, the shear stress decreased at point C2 (because the spur dike armors this point) from 1.47 to 0.51 kPa (Figure 18), with a reduction by a factor of three. However, the possibility of sedimentation increases in this area due to the lower shear stresses. This process causes the gradual modification of the riverbank on the left. In addition, the shear stresses are 9.11 and 12.27 kPa at points C3 and C4, respectively, when the spur dike is placed. This shows increases of 270% and 386% in comparison to the condition without the spur dike. Such a situation occurs due to the presence of an area with maximum velocities near the nose of the spur dike and the flow separation from the structure. In these conditions, scouring occurs around the nose of the spur dike and the eroded area would develop downstream of the structure, which is a result also obtained by Jafari and Sui [42].

At the downstream points, and in particular at points D5 and D6 (Figure 19), the shear stresses are, in presence of a spur dike, 6.34 and 4.66 kPa, respectively. In the case of the absence of the spur dike, the shear stresses at the above points decrease by 161% and 86%. Indeed, when a spur dike is placed, a more significant part of the main flow is directed to the intake, which faces the high-velocity flow in the river. Points D5 and D6 are located along the downstream wall of the intake. This area is characterized by lower shear stresses in comparison to the central and upstream transects due to the direction of the flow toward the intake channel. However, the shear stress at point D3 is almost equal in both cases with and without a spur dike, being about 2 kPa (Figure 19). Meanwhile, this point is located in the river center and downstream of the intake inlet. In other words, the surrounding area is not much affected by the spur dike and the lateral intake, which would explain the almost equal values of the shear stress in both cases.

At the upstream points, in particular points U6 and U5, the values of the shear stress, in the case of the presence of the spur dike, are 15.39 and 14.70 kPa, respectively (Figure 20), whereas, in the case of the absence of the spur dike, both values are about 3.5 kPa, which would show a notable decrease. However, these results are in contrast with those for points

U1 and U2, where the shear stresses in the presence of a spur dike are even smaller than those found in the case without a spur dike. Actually, the presence of the spur dike would cause the surrounding area of points U1 and U2 to be included in the region where the main flow impacts the spur dike, with a significant reduction in the flow velocities and shear stresses.

3.5. Comparison of Results with Previous Similar Literature Studies

Patel et al. [43] found, experimentally, that the maximum local scour occurs at the leading edge of the spur dike; the present research also achieved the same results, though in terms of shear stresses. Karami et al. [28] showed, through a 3D Computational Fluid Dynamic (CFD) code, that placing the spur dike and submerged vanes in the main channel and in front of the intake inlet would increase shear stresses near the base of the vanes and spur dikes themselves. This outcome also complies with the results of the present study. In addition, by comparing the effects of changing the relative spur dike length (i.e., L_S/W_c = 0.20, 0.25, and 0.30, with L_S being spur dike length and W_c the channel width) on the intake efficiency, Karami et al. [28] found that the spur dike with an L_S/W_c = 0.20 allowed a diversion ratio from the initial value of 11% (without dikes and vanes) to 22.2%, with a simultaneous reduction in sedimentation. Iqbal and Tanaka's [40] experimental findings revealed that elongating the spur dike wing length reciprocally affected the depth-averaged velocity (at the spur dike head and near the adjacent spur dike bank), concurrently impacting the flow deflection and backwater rising. Therefore, the general results of these studies are similar, and the presence of a spur dike on the bank opposite the intake inlet would increase the efficiency of the intake structures. They further highlighted that increasing the spur dike length would cause a decrease in the diverted discharge. Conversely, the results of the present study showed that, when placing the longest spur dike, the inflow velocity at the intake inlet increases by 11% in comparison to the shortest spur dike. Actually, Karami et al. [28] considered a spur dike just upstream of the intake inlet and placed perpendicular to the flow. In such a condition, increasing the spur dike length would direct the main flow towards the upstream intake wall, so less flow enters the intake structure. Further, the results of this research showed that the breakwater induced by the spur dike increases the shear stresses for the flow entering the intake structure. However, these findings are in contrast with those obtained by Karami et al. [28], who used parallel and zig-zag submerged vanes at angles of 10 and 30 degrees. Submerged vanes reduce the incoming shear stresses because these plates are placed before the water intake opening. In the present research, the spur dike can divert the main flow and the high-speed areas towards the intake structure. Regarding the development of vortices and their positioning, as well as the generation of low- and high-velocity regions, the results of this study were consistent with the results of earlier research such as that by Tripathi and Pandey [39] (experimental and numerical study), Abbasi et al. [38] (numerical study), and Koken and Constantinescu [41] (experimental and numerical study).

Interestingly, the streamlines around the spur dikes in Flow-3D numerical modelling appear to be in harmony with the experimental evidence reported in some experimental studies on local scour at spur dikes (e.g., Pandey et al. [44] and Aung et al. [45]). As mentioned earlier, in this study, the erosion and sedimentation processes are only presumed to be closely connected with the kinematic fields and/or shear stresses. However, in-depth analysis and comparison between the numerical results of this research and the experimental outcomes regarding the bed morphological changes around spur dikes could lead to further validations.

4. Conclusions

This study was aimed to increase the efficiency and inflow at the lateral intake as well as to reduce the sedimentation area at the intake inlet. To this purpose, the effect on the flow patterns of a spur dike is verified by performing numerical simulations. Three spur dike locations, four spur dike lengths, and five spur dike deflection angles were investigated.

The results generally showed that there are no noticeable changes in the kinematic field of the flow entering the intake when changing the spur dike position. According to the findings, the flow velocities at the intake inlet are directly related to the spur dike length. In particular, the inlet flow velocity increases with an increase in the L_S/B_r, where L_S is the effective spur dike length and B_r is the river width. The longest spur dike, in comparison to the shortest one, would increase the flow velocity at the intake inlet by 11%. In the comparison of four different lengths, the highest inlet velocities were found for the values of L_S/B_r equal to 0.40 and 0.46 (scenarios 3 and 4), with values of 1.55 m/s (V/V_{max} = 0.98) and 1.58 m/s (V/V_{max} = 1.00). The average velocity at point 3 and for the case with L_S/B_r = 0.24 was found to be equal to 0.52 m/s (V/V_{max} = 0.33). In the case of a longer spur dike with L_S/B_r = 0.46, the velocity at the same point was found to be equal to 1.55 m/s (V/V_{max} = 0.98), with an increase of 198%. On the other hand, the results showed that the inlet flow velocity did not change much with the changing of the spur dike deflection angle between 75 and 135 degrees. However, the flow depth at the intake inlet increased by 9% when the spur dike was placed with a deflection angle of 135 degrees in comparison to 75 degrees. Based on the shear stress results, it was found that, in all scenarios, the highest shear stresses were related to the centerline of the river. Also, the shear stress in front of the intake inlet (point C5), in the case of the presence of a spur dike, was found to be equal to 12.63 kPa and, in comparison to the case without a spur dike, increased by 454%. Similarly, at the intake inlet (point C6), the shear stress increased by 50% in the case of the presence of a spur dike. Conversely, in the case of point C2, the spur dike reduced the shear stress from 1.47 to 0.51, with a decrease of 188%. Finally, for the longest spur dike (L_S/B_r = 0.46) and for the deflection angle of 135 degrees, the main flow of the river is directed towards the intake structure with the highest velocity and depth and in the best way. Also, the risk of sediment settling is reduced due to the increased flow velocity towards the intake structure. Hence, the flow intensity in the intake channel increases, and the required flow at the pumping station is supplied. However, the latter configuration could not be the optimal one among all the possible combinations (not all examined in this study) for the placement, length, and deviation angle of the spur dike. Moreover, there are further design configurations (for instance: spur dike of different shape, permeable spur dike, submerged spur dikes or vanes, spur dikes in cascade) which can be considered to further narrow down the search for optimal spur dike design. On the other hand, in the case of the placement of the main spur dike, the shear stress at the intake inlet would increase by 50% in comparison to the case without a spur dike, and this indicates the effect of the spur dike in increasing the flow entering the intake inlet. All the results showed that the placement of a simple spur dike in front of the intake opening would increase the velocities and shear stresses of the flow entering the lateral intake. This is very practical in increasing the water diversion ratio and reducing the possibility of sedimentation at the intake inlet and inside the intake channel. All of these results are possible through the use of hydraulic works of moderate size and cost (in this specific case the use of spur dikes) to enhance the hydraulic efficiency of lateral intakes without (or with little) maintenance over time. An accurate numerical simulation could reveal attractive details for a good functionality even in periods of water scarcity. However, only low ordinary flow conditions were considered here. Future in-depth analyses could consider the impact of the spur dike on the bed morphological changes (e.g., scouring phenomena and aggradation patterns) when floods occur. The design proposals resulting from this study will see their realization in the near future. Therefore, a comparison between numerical results and empirical evidence can only be discussed in a subsequent paper. In this study, only a qualitative and partial comparison with the literature was made possible. On the other hand, the results here presented appear to have the potential of possible extension to other real-word river engineering projects. They are mainly based on numerical simulations which can be applied in similar contexts, but, in any case, would require selected field data for calibration and validation. When 3D processes show potential to become significant, experiments on physical models could be of important help.

Author Contributions: Conceptualization: All authors; Methodology: All authors; Software: S.A.C. and J.A.; Validation: All authors; Formal Analysis: All authors; Investigation: All authors; Resources: All authors; Data Curation: All authors; Writing—Original Draft Preparation: S.A.C., H.A.N. and J.A.; Writing—Review and Editing: All authors; Visualization: All authors; Supervision: G.O., M.V. and J.A.; Project Administration: G.O., M.V. and J.A.; Funding Acquisition: J.A. and S.M.S. All authors have read and agreed to the published version of the manuscript.

Funding: This work was supported by the Shahid Chamran University of Ahvaz and Khuzestan Water and Power Authority.

Data Availability Statement: All data generated or analysed during this study are available from the corresponding authors on request.

Acknowledgments: The authors are grateful to the Research Council of the Shahid Chamran University of Ahvaz, the Khuzestan Water and Power Authority (KWPA), and the Center of Excellence of the Irrigation and Drainage Networks Improvement and Maintenance (Ahvaz, Iran) for their valuable support.

Conflicts of Interest: The authors declare no conflicts of interest.

References

1. Tadda, M.A.; Ahsan, A.; Imteaz, M.; Shitu, A.; Danhassan, U.A.; Muhammad, A.I. Operation and Maintenance of Hydraulic Structures. In *Hydraulic Structures—Theory and Applications*; Ahsan, A., Ed.; IntechOpen: London, UK, 2020. [CrossRef]
2. Montaseri, H.; Tavakoli, K.; Evangelista, S.; Omidvar, P. Sediment transport and bed evolution in a 180° curved channel with lateral intake: Numerical simulations using Eulerian and Discrete Phase models. *Int. J. Mod. Phys. C* **2020**, *31*, 2050113. [CrossRef]
3. Moghadam, M.K.; Keshavarzi, A.R. An optimised water intake with the presence of submerged vanes in irrigation canals. *Irrig. Drain.* **2010**, *59*, 432–441. [CrossRef]
4. Alomari, N.K.; Yusuf, B.; Mohammad, T.A.; Ghazali, A.H. Influence of diversion angle on water and sediment flow into diversion channel. *Int. J. Sediment Res.* **2020**, *35*, 600–608. [CrossRef]
5. Masjedi, A.; Foroushani, E.P. Experimental effect of flow depth on ratio discharge in lateral intakes in river bend. *IOP Conf. Ser. Earth Environ. Sci.* **2012**, *15*, 062054. [CrossRef]
6. Farshad, R.; Kashefipour, S.M.; Ghomeshi, M.; Oliveto, G. Temporal scour variations at permeable and angled spur dikes under steady and unsteady flows. *Water* **2022**, *14*, 3310. [CrossRef]
7. Montaseri, H.; Asiaei, H.; Baghlani, A.; Omidvar, P. Numerical study of flow pattern around lateral intake in a curved channel. *Int. J. Mod. Phys. C* **2019**, *30*, 1950083. [CrossRef]
8. Neary, V.S.; Odgaard, A.J. Three-dimensional flow structure at open-channel diversions. *J. Hydraul. Eng.* **1993**, *119*, 1223–1230. [CrossRef]
9. Jalili, H.R.; Dalir, A.H.; Farsadizadeh, D. Effect of mouth shape on the flow pattern and sedimentation in the vertical lateral diversion. *Water Soil* **2012**, *25*, 1321–1331.
10. Al-Zubaidy, R.A.; Ismaeil, R.H. Sediment control at the lateral channel inlet. *IOP Conf. Ser. Earth Environ. Sci.* **2022**, *961*, 012096. [CrossRef]
11. Abolghasemi, M.; Ghodsian, M.; Sanginabadi, H. The effect of flow diversion on sediment entering intake located at section 52° in sinuous rivers. *J. Hydraul.* **2011**, *6*, 41–52.
12. Kashyap, S.; Constantinescu, G.; Rennie, C.D.; Post, G.; Townsend, R. Influence of channel aspect ratio and curvature on flow, secondary circulation, and bed shear stress in a rectangular channel bend. *J. Hydraul. Eng.* **2012**, *138*, 1045–1059. [CrossRef]
13. Azimi, H.; Shabanlou, S.; Kardar, S. Flow field within rectangular lateral intakes in the subcritical flow regimes. *Model. Earth Syst. Environ.* **2019**, *5*, 421–430. [CrossRef]
14. Babagoli Sefidkoohi, R.; Shahidi, A.; Ramezani, Y.; Kahe, M. Simulation of flow pattern in intake by using a numerical model. *Water Harvest. Res.* **2017**, *2*, 24–36.
15. Safarzadeh, A.; Khaiatrostami, B. Mean flow characteristics, vertical structures and bed shear stress at open channel bifurcation. *J. Appl. Res. Water Wastewater* **2017**, *4*, 299–304.
16. Tavakoli, K.; Montaseri, H.; Omidvar, P.; Evangelista, S. Numerical simulation of sediment transport in a U-shaped channel with lateral intake: Effects of intake position and diversion angle. *Int. J. Mod. Phys. C* **2019**, *3*, 1950071. [CrossRef]
17. Sayed, T. An experimental study of branching flow in open channels. *Limnol. Rev.* **2019**, *19*, 93–101. [CrossRef]
18. Heidari Rad, P.; Kamanbedast, A.; Heidarnejad, M.; Masjedi, A.; Hasonizadeh, H. The effect of convergence and divergence on flow pattern and sediment transport in lateral intakes using physical and numerical models. *Ain Shams Eng. J.* **2020**, *11*, 445–454. [CrossRef]
19. Meshkati, S.M.; Salehi, S. Numerical simulation of 3D flow pattern at lateral intake in 180-degree bend. *Iran. J. Soil Water Res.* **2021**, *52*, 37–51.
20. Niknezhad, F.; Mahmoudi, A.; Vaghefi, M. A Study of the effects of a lateral intake's positions on the flow pattern around a bridge pier in a 180° bend using SSIIM2. *Arab. J. Sci. Eng.* **2023**, *48*, 12903–12929. [CrossRef]

21. Davoodi, L.; Bejestan, M.S. Control of sediment entry to intake on a trapezoidal channel by submerged vane. *Ecol. Environ. Conserv.* **2012**, *18*, 165–169.
22. Sarhadi, A.; Jabbari, E. Investigating effect of different parameters of the submerged vanes on the lateral intake discharge located in the 180 degree bend using the numerical model. *J. Civ. Eng.* **2017**, *3*, 1176–1187. [CrossRef]
23. Firozjaei, R.M.; Salehi Neyshabouri, S.A.A.; Amini Sola, S.; Mohajeri, S.H. Numerical simulation on the performance improvement of a lateral intake using submerged vanes. *IJST Trans. Civ. Eng.* **2019**, *43*, 167–177.
24. Baltazar, J.; Alves, E.; Bombar, G.; Cardoso, H.A. Effect of a submerged vane-field on the flow pattern of a movable bed channel with a 90° lateral diversion. *Water* **2021**, *13*, 828. [CrossRef]
25. Moghadam, M.K.; Amini, A.; Keshavarzi, A. Intake design attributes and submerged vanes effects on sedimentation and shear stress. *Water Environ. J.* **2019**, *34*, 374–380. [CrossRef]
26. Shamloo, H.; Asnaashari, A.; Pirzadeh, B. Numerical investigation of the effects of submerged vanes and spur dikes on sediment control at lateral intakes. In Proceedings of the 12th Annual Conference of Thai Society of Agricultural Engineering "International Conference in Agricultural Engineering" (Novelty, Clean and Sustainable) Chon-Chan Pattaya Resort, Chonburi, Thailand, 31 March–1 April 2011.
27. Daneshfaraz, R.; Bagheri, Y.; Ghaderi, A.; Ghahremanzadeh, A. An analysis of flowing pattern around T-shaped spur dike at 90° arc, based on Fluent and Flow-3D models. *Int. J. Water Resour. Dev.* **2015**, *3*, 1–9.
28. Karami, H.; Farzin, S.; Sadrabadi, M.T.; Moazeni, H. Simulation of flow pattern at rectangular lateral intake with different dike and submerged vane scenarios. *Water Sci. Eng.* **2017**, *10*, 246–255. [CrossRef]
29. Geravandi, E.; Kamanbedast, A.A.; Masjedi, A.R.; Heidarnejad, M.; Bordbar, A. Laboratory investigation of the impact of armor dike simple and L-shaped in upstream and downstream intake of the hydraulic flow of the Kheirabad River to help physical model. *Fresenius Environ. Bull.* **2018**, *27*, 263–276.
30. Zamani, M.; Rabiefar, H.; Rostami, M. Experimental evaluation of spur dikes placement position effect on the hydraulic and erosion conditions of intakes. *Water Supply* **2020**, *20*, 900–908. [CrossRef]
31. Moradinejad, A.; Saneie, M.; Ghaderi, A.; Zamanieh Shahri, S.M. Experimental study of flow pattern and sediment behavior near the intake structures using the spur dike and skimming wall. *Appl. Water Sci.* **2019**, *9*, 195. [CrossRef]
32. Ahadiyan, J.; Chenari, S.A.; Nadian, H.A.; Katopodis, C.; Valipour, M.; Sajjadi, S.M.; Omidvarinia, M. Sustainable systems engineering by CFD modeling of lateral intake flow with flexible gate operations to improve efficient water supply. *Int. J. Sediment Res.* **2024**, *in press*. [CrossRef]
33. Hirt, C.W.; Nichols, B.D. Volume of Fluid (VOF) method for the dynamics of free boundaries. *J. Comput. Phys.* **1981**, *39*, 201–225. [CrossRef]
34. Di Francesco, S.; Biscarini, C.; Manciola, P. Numerical simulation of water free-surface flows through a front-tracking lattice Boltzmann approach. *J. Hydroinform.* **2015**, *17*, 1–6. [CrossRef]
35. Daneshfaraz, R.; Aminvash, E.; Bagherzadeh, M.; Ghaderi, A.; Kuriqi, A.; Najibi, A.; Ricardo, A.M. Laboratory investigation of hydraulic parameters on inclined drop equipped with fishway elements. *Symmetry* **2021**, *13*, 1643. [CrossRef]
36. Ghaderi, A.; Abbasi, S.; Di Francesco, S. Numerical study on the hydraulic properties of flow over different pooled stepped spillways. *Water* **2021**, *13*, 710. [CrossRef]
37. Knight, D.W.; Omran, M.; Tang, X. Modeling depth-averaged velocity and boundary shear in trapezoidal channels with secondary flows. *J. Hydraul. Eng.* **2007**, *133*, 39–47. [CrossRef]
38. Abbasi, S.; Kamanbedast, A.; Ahadian, J. Numerical investigation of angle and geometric of L-shape groin on the flow and erosion regime at river bends. *World Appl. Sci. J.* **2011**, *15*, 279–284.
39. Tripathi, R.P.; Pandey, K.K. Scour around spur dike in curved channel: A review. *Acta Geophys.* **2022**, *70*, 2469–2485. [CrossRef]
40. Iqbal, S.; Tanaka, N. Hydraulic performance assessment of various submerged pile designs around an emerged dike. *Water Sci. Eng.* **2024**, *in press*. [CrossRef]
41. Koken, M.; Constantinescu, G. An investigation of the flow and scour mechanisms around isolated spur dikes in a shallow open channel: 1. Conditions corresponding to the initiation of the erosion and deposition process. *Water Resour. Res.* **2008**, *44*, W08406. [CrossRef]
42. Jafari, R.; Sui, J. Velocity field and turbulence structure around spur dikes with different angles of orientation under ice covered flow conditions. *Water* **2021**, *13*, 1844. [CrossRef]
43. Patel, H.K.; Qi, M.; Kumar, B. Downward seepage effects on flow near a L-shape spur dike and bed morphology. *Int. J. Sediment Res.* **2024**, *39*, 194–208. [CrossRef]
44. Pandey, M.; Valyrakis, M.; Qi, M.; Sharma, A.; Lodhi, A.S. Experimental assessment and prediction of temporal scour depth around a spur dike. *Int. J. Sediment Res.* **2021**, *36*, 17–28. [CrossRef]
45. Aung, H.; Onorati, B.; Oliveto, G.; Yu, G. Riverbed morphologies induced by local scour processes at single spur dike and spur dikes in cascade. *Water* **2023**, *15*, 1746. [CrossRef]

Disclaimer/Publisher's Note: The statements, opinions and data contained in all publications are solely those of the individual author(s) and contributor(s) and not of MDPI and/or the editor(s). MDPI and/or the editor(s) disclaim responsibility for any injury to people or property resulting from any ideas, methods, instructions or products referred to in the content.